Research Article

Structural and thermal properties of pure and chromium doped zinc oxide nanoparticles

Ababay Ketema Worku[1] · Delele Worku Ayele[1,2] · Nigus Gabbiye Habtu[1,3] · Getu Alemayehu Melas[1] · Temesgen Atnafu Yemata[3] · Negese Yayu Mekonnen[1] · Minbale Admas Teshager[4]

Received: 23 March 2021 / Accepted: 1 June 2021
Published online: 13 June 2021
© The Author(s) 2021 OPEN

Abstract

Pure ZnO and Cr-doped ZnO nanoparticles have been synthesized via a facile chemical co-precipitation route and their structural, thermal characteristics were discussed systematically. In the experimental producer, the doping concentration has varied the range, 0.05–0.1 M, while calcined at 600 °C. The influence of Cr-doping on the physical characteristics of ZnO nanoparticles was investigated and addressed. As-prepared samples were analyzed via XRD, FTIR, TGA/DTA, BET, and ICP-MS. XRD analysis shows that ZnO and Cr doped ZnO nanoparticles with average particle sizes between 23 and 39 nm were successfully developed with hexagonal wurtzite structure. The FTIR spectroscopy analysis confirms the existence of chromium in the doped ZnO nanoparticles and the formation of ZnO. The TGA/DTA analysis shows that Cr–ZnO nanoparticles are more thermally stable than ZnO nanoparticles. Moreover, the dopant concentration has been analyzed via ICP-MS and showed a good agreement with the expected chromium concentration. The BET surface area measurement shows that 176.25 m^2/g and 287.17 m^2/g for un-doped ZnO, and 0.1 M Cr-doped ZnO nanoparticles, respectively. Hence, doping of Cr enhances the surface area and thermal stability. Thus, Cr–ZnO nanoparticles show good thermal stability, and high surface area, which is an excellent characteristices of nanomaterials.

✉ Delele Worku Ayele, Delel.worku@bdu.edu.et; ✉ Nigus Gabbiye Habtu, nigus.gabiye@bdu.edu.et | [1]Bahir Dar Energy Center, Bahir Dar Institute of Technology, Bahir Dar University, P.O. Box 26, Bahir Dar, Ethiopia. [2]Department of Chemistry, Bahir Dar University, P.O. Box 79, Bahir Dar, Ethiopia. [3]Department of Chemical Engineering, Bahir Dar Institute of Technology, Bahir Dar University, P.O. Box 26, Bahir Dar, Ethiopia. [4]Department of Chemistry, Debre Markos University, P.O. Box 269, Debre Markos, Ethiopia.

Graphic abstract

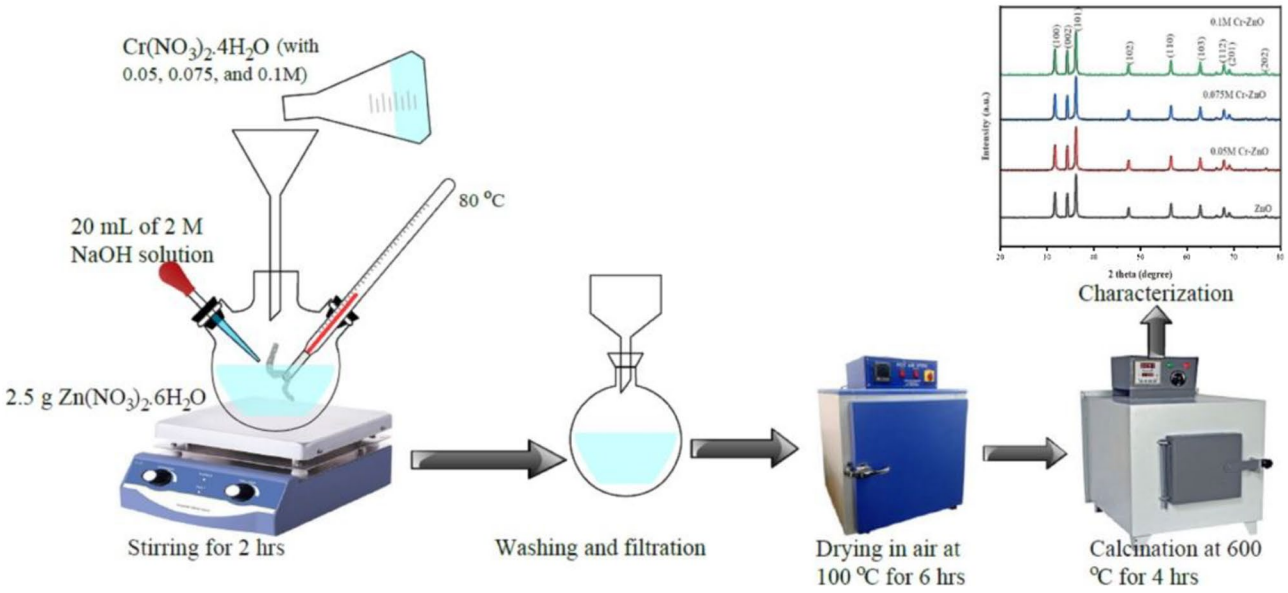

Highlights

- Pure ZnO and Cr–ZnO nanoparticles have been synthesized using a facile and cost effective technique.
- The as prepared samples of pure ZnO and Cr–ZnO nanoparticles show wurtzite structure.
- Cr doped ZnO nanoparticles showed a higher surface area than that of un-doped ZnO nanoparticles.
- The synergetic effect of Cr and ZnO nanoparticles attributed to good thermal stability and high surface area.

Keywords Chromium · Zinc oxide · Thermal stability · Co-precipitation

1 Introduction

Recently, nanoscale materials have revealed advanced occasions for several technological utilization [1–3]. Because of their unique, optical, catalytic, electrical, and magnetic characteristics and enhanced physical characteristics such as thermal, or chemical and mechanical, metal oxide nanoparticles are widely employed for many applications like magnetic materials, cosmetics, batteries, pharmaceuticals, catalysts, optical devices, protective coatings structured materials, and biomaterials [4–7]. Thus, the preparation of metal oxide semiconductors with different sizes and morphology has gained significant attention due to their excellent chemical stability and thermal property [8–11]. Among different nanomaterials, ZnO nanoparticles (NPs) have been extensively employed in many industrial sectors such as electro-optical devices, gas sensors, photocatalysts, antimicrobial agents, antibiotics, and electrode materials [12–15]. ZnO can be obtained in different crystallized forms such as rock salt, zincblende, and wurtzite with a corresponding cubic, cubic, and hexagonal structure, respectively. Among these structures, wurtzite is the most stable and thus most popular at ambient circumstances [16–18]. Hence, numerous efforts have been utilized in the preparation of ZnO nanoparticles with the variation in size and morphology [5, 19, 20]. Recent studies indicate that magnetic, optical, electrical, and structural characteristics of ZnO NPs can be managed by defect engineering of ZnO lattice [21]. Furthermore, we can adjust the characteristics of ZnO NPs for aspired utilization via managing structure, shape, and morphology [22, 23]. From different strategies doping of different materials in ZnO nanoparticles shows remarkable changes in its property [24, 25]. The doping of selective elements will change its electronic structure, and then affect the catalytic, optical, and structural characteristics [26]. In terms of metal doping with different concentrations, the structure, morphology, and optical properties of ZnO nanocrystals were studied. To change the bandgap, various techniques are utilized, among which the doping of transition metal ions is important [27, 28]. Hence,

the doping of ZnO nanoparticles with transition metals, like Ag, Sb, Cr, Mn, Fe, P, In, Co, Li, Al, Ga, As, Sn, Mg, etc., have been observed to perform fine control of morphology and size [29–31]. From the various transition metals, Ag ions have been taken as dopants, due to their simple link matrices, and high-corrosion resistance as well as their hardness [32–35]. Furthermore, among the various transition metals, Cr ions have been gained great attention as a dopant due to their Cr^{3+} radius, which is closer to that of Zn^{2+}. Hence, Cr^{3+} can simply dope with the ZnO crystal lattice or replace the site of Zn^{2+} in ZnO [36]. The purpose of this study is to examine the impact of Cr doping in structural and thermal characteristics of ZnO NPs [37–39]. There are various methods for the development of ZnO and Cr doped ZnO like sol–gel method, chemical coprecipitation, microemulsion, thermal decomposition, spray pyrolysis, electrochemical deposition, and hydrothermal, solid-state reaction techniques have been utilized mostly [40–42]. Hence, cost-effective, low-temperature, fast, simple, and scalable synthesis methods are preferable for the preparation of NPs [43, 44]. Among these, a simple and low-cost chemical co-precipitation route has been selected for the synthesis of ZnO and Cr doped ZnO nanoparticles from zinc nitrate hexahydrate and chromium acetate tetrahydrate using sodium hydroxide as a precipitating agent [45, 46]. The advantages of the chemical co-precipitation technique from others for preparing nanoparticles are to obtain smaller particle size, pure particles, and better homogeneity [47–49]. In this work, the development of ZnO and Cr doped ZnO nanoparticles have been reported via a simple and low-cost route. Thus, the prepared products have been analyzed via XRD, FTIR, TGA/DTA, BET, and ICP-MS. In the analysis Cr, doped ZnO nanoparticles show better thermal stability and high surface area.

2 Materials and methods

2.1 Materials

In this work the chemicals utilized were analytical grade and used without further refinement. Zinc nitrate hexahydrate ($Zn(NO_3)_2{\cdot}6H_2O$), sodium hydroxide (NaOH), ethanol, and chromium nitrate tetrahydrate ($Cr(NO_3)_2{\cdot}4H_2O$) were obtained from Merck Limited, India. Deionized was used as a solvent.

2.2 Preparation of ZnO and Cr-doped ZnO

In this work, nanoparticles of pure and Cr doped ZnO with 0.05, 0.075, and 0.1 M of Cr, have been prepared via co-precipitation approach using zinc nitrate hexahydrate, sodium hydroxide (NaOH) and chromium acetate tetrahydrate as precursor materials. For synthesis of Cr-doped ZnO NPs, 2.5 g of zinc nitrate hexahydrate was dissolved in 80 ml deionized water and (0.05, 0.075, and 0.1 M) amount chromium acetate tetrahydrate dissolved in 100 ml was added to the above solution. 20 mL of 2 M NaOH solution was slowly added into the starting materials under vigorous stirring until pH of the solution become 12. The solution acquired was stirred for 2 h at 80 °C. The obtained product were filtered and washed for several times with deionized water and ethanol to remove the impurities. The as-prepared nanoparticles were dried in air at 100 °C for 6 h. Finally, Annealing of the product was provided out at 600 °C for 4 h. The samples were calcined at 600 °C for 4 h, due to energy from the heat would improve the vibration and diffusion of the atoms in the lattice, thereby crystallizing the atoms. The experimental setup and additional explanations of the systems are shown in Fig. 1.

2.3 Characterization

The thermal characteristics of as-prepared materials are analyzed by TGA and DTA. Structural properties of ZnO and Cr–ZnO nanoparticles was examined via XRD (SHIMADZU, MAXima_X XRD-7000) with Cu-K_α radiation in the theta-2theta angle range of 20° and 80°. The functional groups and other impurities exist in of ZnO and Cr–ZnO nanoparticles have been analyzed via Fourier Transform Infrared spectroscopy (FTIR) (JASCO MODEL FT-IR 6660) in the wavelength range of 400–4000 cm^{-1}. The Brunauer–Emmett–Teller (BET) technique was conducted to estimate the total surface area of as-prepared nanomaterial using Quanta chrome Instruments version 11.0. Inductively coupled plasma mass spectrometry (ICP-MS, Agilent 7500A) was used to analyse the concentration of residual doping elements in the mixture at the end of the preparation. Before testing, a strong acid solution has been used to dissolve all samples.

3 Results and discussion

3.1 Structural analysis

The XRD patterns of pure ZnO and Cr doped ZnO nanoparticles are illustrated in Fig. 2. As shown in Fig. 2, all the diffraction peaks detected at 2θ values of 31.71°, 34.36°, 36.18°, 47.46°, 56.56°, 62.76°, 67.88°, 69.03°, and 76.91° matched well to the (100), (002), (101), (102), (110), (103), (112), (201),and (202), planes, respectively, for hexagonal ZnO (JCPDS 01-076-0704). Thus, the peaks observed from ZnO nanoparticles are matched with the wurtzite structure [50, 51]. From the XRD analysis there are no diffraction peaks belonging to Cr species like Cr metal, and Cr oxides

in as prepared nanoparticles. The result shows that all Cr ions were perfectly incorporated into the lattice sites of the crystals, the products consist of pure phase, and no other impurities characteristic peaks are observed. The average crystallite size, *D*, of ZnO and Cr doped ZnO nanoparticles were calculated via the Scherrers equation [52, 53]:

$$D = \frac{K\lambda}{\beta cos\theta} \quad (1)$$

where "*K*" is the Scherer constant, "*λ*" is the wavelength of the radiation sources, "*β*" is the full width at the half maximum intensity (FWHM) and "*θ*" is the peak position. Hence the average crystallites size of pure ZnO, 0.05 M Cr–ZnO, 0.07 M Cr–ZnO, and 0.1 M Cr–ZnO was 39 nm, 31 nm, 27 nm, 23 nm, respectively. When the doping concentration of chromium increases the average crystallite size (D) decreases, because of the distortion in the host ZnO lattice via Cr^{3+} ions. In addition, the strain formed in the samples because of Cr doping has been computed using following equation [53]:

$$Micro - strain(\varepsilon) = \frac{\beta cos\theta}{4} \quad (2)$$

where "*ε*" is strain and "*θ*" is the Bragg's angle in degrees. Moreover, the dislocation density (*δ*) values of as-prepared samples were determined using the following equation, which is tabulated in Table 1 [53].

$$\delta = 1/D^2 \quad (3)$$

where "*δ*" is the dislocation density and "D" is the crystallites size. The value of dislocation density was seen to be increased as the dopant increases (Table 1). Therefore, the XRD spectra of pure and doped ZnO NPs shows that Cr^{3+} ions are exist within the lattice structure of ZnO via substituting certain Zn^{2+} ions from its lattice position without forming chromium-related oxide phases. Moreover, the radius of Zn^{2+} ion (0.74 A°) is different from the radius of Cr^{3+} ion (0.63 A°), and this variation in ion radius size will cause internal lattice strain within the lattice structure of Cr^{3+} ion doped ZnO NPs. The internal lattice micro-strain of the Cr^{3+} ion-doped ZnO nanoparticles is larger than that of the pure ZnO NPs. As the percentage of Cr^{3+} ion doping in the ZnO structure increases, they gradually increase.

3.2 BET surface area analysis

The BET technique was conducted to estimate the total surface area of the as-prepared nanoparticles. The surface area of ZnO and Cr doped ZnO nanoparticles at different dopant concentration was estimated. The results concerning BET surface area shows a dramatically change increment in surface area due to Cr-doping. The BET surface area measurement shows of un-doped ZnO and 0.1 M Cr-doping ZnO nanoparticles are shown in Table 1. The BET surface area result shows that the prepared nanomaterials with high surface area. Thus, as approved by XRD analysis, crystallite size diminishes; consequently, the surface area grows. Hence, improving the porosity of the surface increases the surface area of nanoparticles. Therefore, higher surface area formation in the doped nanoparticles may be accredited to the thermal decomposition of Cr species during calcination process [6, 54].

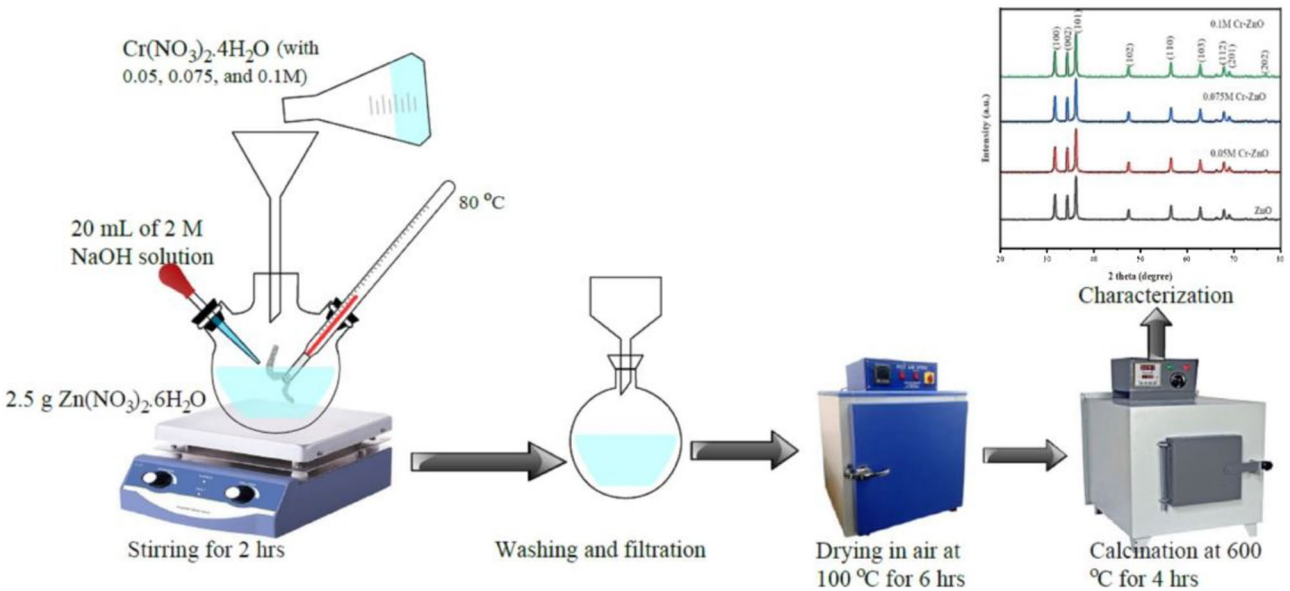

Fig. 1 Schematic illustration of Cr-doped ZnO nanoparticles synthesis by chemical co-precipitation route

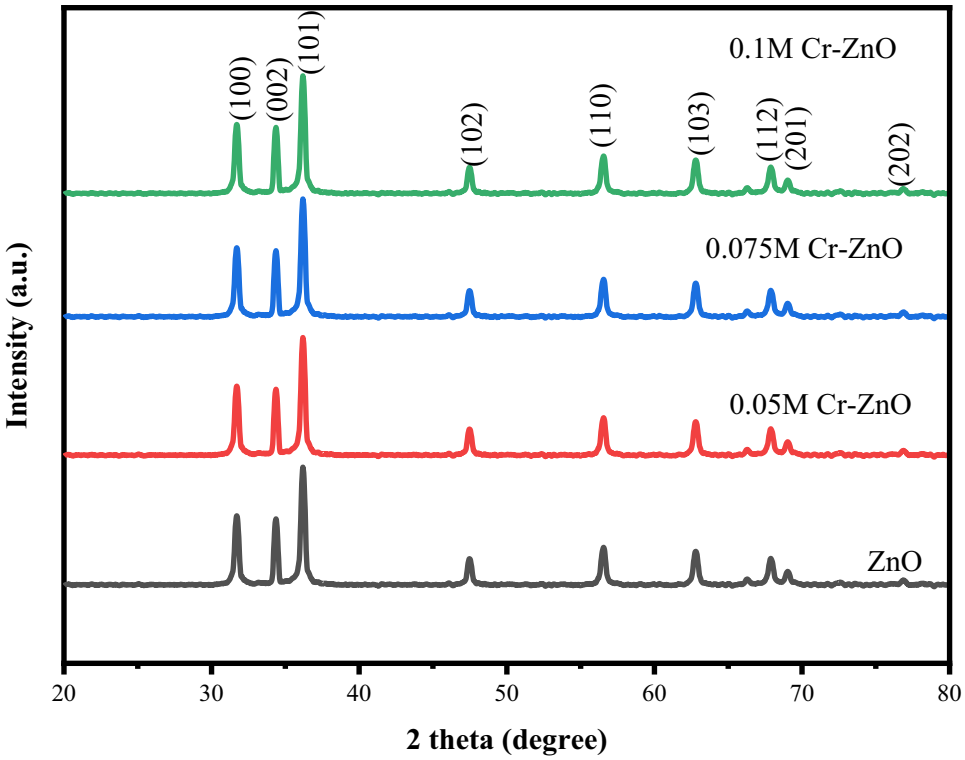

Fig. 2 XRD patterns for ZnO, and Cr doped ZnO nanoparticles

3.3 Dopant concentration analysis

The amount of chromium incorporated into ZnO NPs ware analysed using inductively coupled plasma mass spectroscopy (ICP-MS). We have prepared various Cr doped ZnO NPs samples to accurately measure the concentration of chromium. Table 2 shows the ICP-MS results of pure ZnO and Cr doped ZnO NPs. As shown in Table 2, there is a very good agreement among the expected chromium percentage using stoichiometry and the actual measured chromium concentration incorporated in the ZnO nanostructures [55].

3.4 Functional group analysis

FTIR spectra of ZnO and Cr–ZnO nanoparticles are illustrated in the Fig. 3. The broad absorption peak located around 3450 and 1643 cm^{-1} shows the stretching and bending vibration of O–H, which emerged from water molecule adsorbed on the surface of as-prepared materials. Additionally, the two strong bands at 1437 and 1076 cm^{-1} in Cr-doped ZnO materials may assigned to the vibration of the Zn–Cr bonds, which shows the successful doping of Cr ion in ZnO nanoparticles. The Zn–O bond is corresponding to the stretching frequency at 483 cm^{-1} for ZnO. Moreover, bands at 880 cm^{-1} may be the stretching vibration of Cr–O. Thus, Cr–O formation confirms the incorporation of the chromium atoms in the ZnO lattice. This shows that the observed shifts in FTIR spectra is because of the incorporation of chromium atoms in the ZnO lattice. FTIR spectra of pure ZnO and Cr doped ZnO nanoparticles investigated in this work are in excellent agreement with previously recorded values [56–58].

Table 1 XRD parameter and specific surface area values of un-doped ZnO and Cr-doped ZnO NPs

Nanomaterials	Average crystalline size *D* (nm)	Micro-strain (10^{-4})	$\delta \times 10^4$ (nm^{-2})	Specific surface area (m^2/g)
ZnO	39	11.5	6.57	176.25
0.05 M Cr–ZnO	31	13.4	10.40	–
0.075 M Cr–ZnO	27	14.2	13.71	–
0.1 M Cr–ZnO	23	15.3	18.90	287.17

3.5 Thermal property analysis

The TGA/DTA analysis was conducted to study the thermal stability of ZnO and Cr–ZnO nanoparticles. Figure 4 illustrates the TGA/DTA curve of ZnO and Cr–ZnO nanoparticles, which was scanned at the rate of 15 °C/min in the range of 30–800 °C under air atmosphere. For pure ZnO nanoparticles, the first weight loss of 2.8% from 25 to 174 °C is because of the evaporation of water molecules on the surface of ZnO nanoparticles. Then, the sample illustrates the second weight loss of 1.97% and a in the range of 174–311 °C, which attributed to the removal of organic components. The final weight loss of 3.63% in the range of 311–540 °C is the crystallization of as-prepared material during the heating process. The crossponding DTA peaks are observed at 345 °C, 402 °C and 464 °C (Fig. 4a). For pure Cr–ZnO nanoparticles, the first weight loss of 1.2% from 25 to 287 °C is because of the evaporation of water molecules on the surface of ZnO nanoparticles. Then, the sample displays the second weight loss of 5.23% and a in the range of 287–480 °C, which attributed to the removal of organic components. The final weight loss of 0.2% in the range of 480–656 °C is the crystallization of as-prepared material during the heating process. The crossponding DTA peaks are observed at 315 °C, 326 °C and 340 °C (Fig. 4b). Hence, TGA analysis showed that total weight loss of 8.13% and 6.63% for ZnO and Cr–ZnO nanoparticles, respectively. Thus, Cr–ZnO nanoparticles are more thermally stable than ZnO [59].

Table 2 Doping concentration of chromium obtained from ICP-MS result

Sample	Expected Cr (formulated composition) (mol%)	ICP-MS Actual content of Cr (mol%)
0.05 M Cr–ZnO	0.5	0.46
0.075 M Cr–ZnO	0.75	0.69
0.1 M Cr–ZnO	1.0	0.97

4 Conclusions

In this paper, ZnO and chromium doped zinc oxide (Cr–ZnO) nanoparticles were developed via a simple chemical co-precipitation route by changing the doping concentration in the range 0.05–0.1 M, which is further calcined at 600 °C. The influence of Cr-doping on the physical characteristics of ZnO nanoparticles was investigated and addressed. Hence, developed samples were examined via XRD, FTIR, TGA/DTA, BET, and ICP-MS. The crystal structure of ZnO and Cr doped ZnO nanoparticles was the hexagonal wurtzite without any additional peaks for all samples regardless of the dopant concentration. However, chromium doping has no noticeable influence on the crystal structure of ZnO as determined by the results of XRD analysis. The FTIR spectroscopy analysis confirms the existence

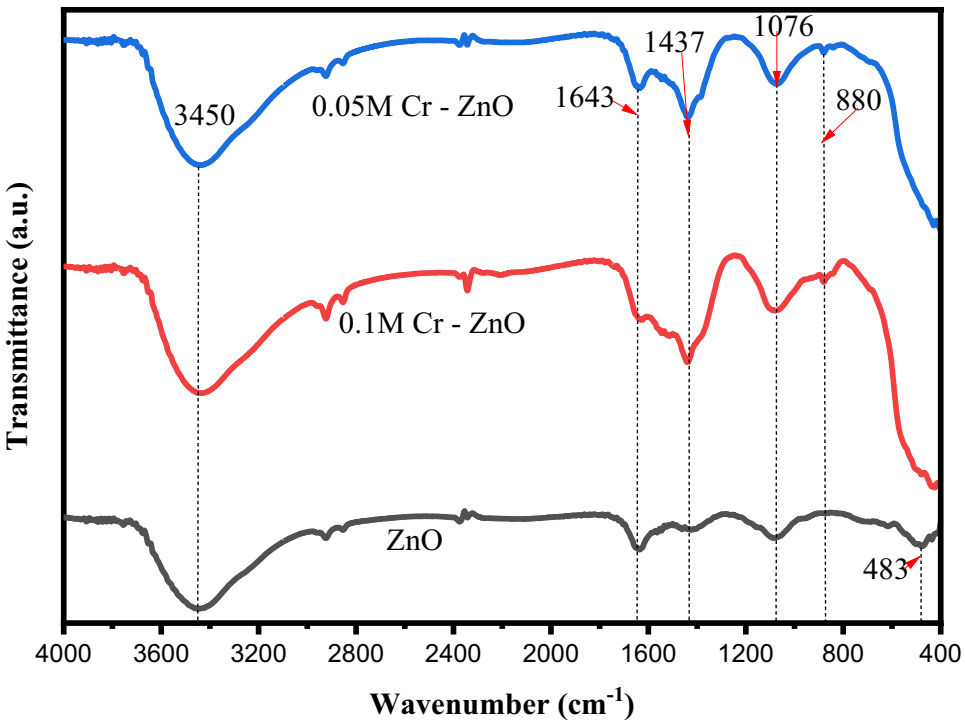

Fig. 3 FTIR spectra of ZnO, and Cr doped ZnO nanoparticles

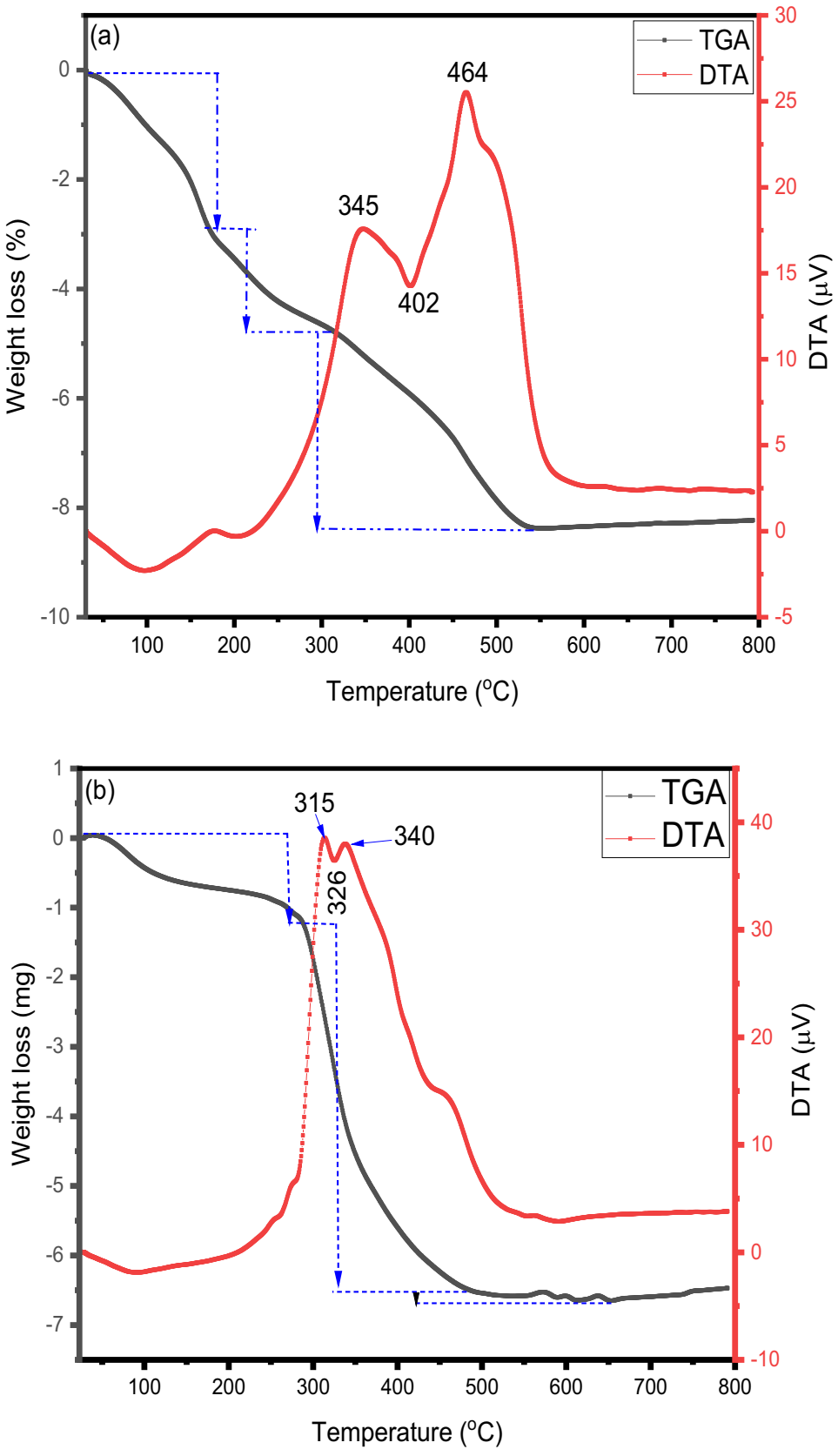

Fig. 4 TGA/DTA illustration of **a** ZnO nanoparticles, and **b** Cr–ZnO nanoparticles

of chromium in the doped ZnO nanoparticles and the formation of ZnO. TGA/DTA analysis shows that Cr–ZnO nanoparticles are more thermally stable than ZnO nanoparticles. In addition, the concentration of the dopant has been analyzed by ICP-MS and showed good agreement with the expected chromium concentration. The BET surface area measurement shows 176.25 m^2/g for un-doped ZnO and 287.17 m^2/g for 0.1 M Cr-doping ZnO nanoparticles. Thus, the addition of chromium in ZnO nanoparticles increases the surface area and thermal stability.

Acknowledgements The authors acknowledge Bahir Dar University, Bahir Technology of Institute, Ethiopia, for providing financial support.

Author contributions AKW was involved in the experiments, data analysis and discussion. GAM, NYM, TAY and MAT drafted the manuscript. DWA and NGH supervised the experiments and edit the final manuscript.

Funding The authors declare that no financial interests.

Declarations

Conflict of interest The authors declare that they have no known competing financial interests or personal relationships that could have appeared to influence the work reported in this paper.

Open Access This article is licensed under a Creative Commons Attribution 4.0 International License, which permits use, sharing, adaptation, distribution and reproduction in any medium or format, as long as you give appropriate credit to the original author(s) and the source, provide a link to the Creative Commons licence, and indicate if changes were made. The images or other third party material in this article are included in the article's Creative Commons licence, unless indicated otherwise in a credit line to the material. If material is not included in the article's Creative Commons licence and your intended use is not permitted by statutory regulation or exceeds the permitted use, you will need to obtain permission directly from the copyright holder. To view a copy of this licence, visit http://creativecommons.org/licenses/by/4.0/.

References

1. Phuruangrat A, Siri S, Wadbua P et al (2019) Microwave-assisted synthesis, photocatalysis and antibacterial activity of Ag nanoparticles supported on ZnO flowers. J Phys Chem Solids 126:170–177. https://doi.org/10.1016/j.jpcs.2018.11.007
2. El Saeed AM, El-Fattah MA, Azzam AM (2015) Synthesis of ZnO nanoparticles and studying its influence on the antimicrobial, anticorrosion and mechanical behavior of polyurethane composite for surface coating. Dye Pigment 121:282–289. https://doi.org/10.1016/j.dyepig.2015.05.037
3. Caregnato P, Espinosa Jiménez KR, Villabrille PI (2020) Ce-doped ZnO as photocatalyst for carbamazepine degradation. Catal Today. https://doi.org/10.1016/j.cattod.2020.07.031
4. Gao P, Ng K, Sun DD (2013) Sulfonated graphene oxide–ZnO–Ag photocatalyst for fast photodegradation and disinfection under visible light. J Hazard Mater 262:826–835. https://doi.org/10.1016/j.jhazmat.2013.09.055
5. Ma J, Liu J, Bao Y et al (2013) Synthesis of large-scale uniform mulberry-like ZnO particles with microwave hydrothermal method and its antibacterial property. Ceram Int 39:2803–2810. https://doi.org/10.1016/j.ceramint.2012.09.049
6. Ahmad I, Akhtar MS, Ahmed E et al (2021) Lu modified ZnO/CNTs composite: a promising photocatalyst for hydrogen evolution under visible light illumination. J Colloid Interface Sci 584:182–192. https://doi.org/10.1016/j.jcis.2020.09.116
7. Xia Y, Gang R, Xu L et al (2020) Nanorod-pillared mesoporous rGO/ZnO/Au hybrids for photocatalytic Cr (VI) reduction: enhanced Cr(VI) adsorption and solar energy harvest. Ceram Int 46:1487–1493. https://doi.org/10.1016/j.ceramint.2019.09.115
8. Basnet P, Chatterjee S (2020) Structure-directing property and growth mechanism induced by capping agents in nanostructured ZnO during hydrothermal synthesis—a systematic review. Nano Struct Nano Obj 22:100426
9. Suwanboon S, Amornpitoksuk P, Sukolrat A, Muensit N (2013) Optical and photocatalytic properties of La-doped ZnO nanoparticles prepared via precipitation and mechanical milling method. Ceram Int 39:2811–2819. https://doi.org/10.1016/j.ceramint.2012.09.050
10. Qi K, Xing X, Zada A et al (2020) Transition metal doped ZnO nanoparticles with enhanced photocatalytic and antibacterial performances: experimental and DFT studies. Ceram Int 46:1494–1502. https://doi.org/10.1016/j.ceramint.2019.09.116
11. Sun Y, Zong Y, Feng J et al (2018) Oxygen vacancies driven size-dependent d0 room temperature ferromagnetism in well-dispersed dopant-free ZnO nanoparticles and density functional theory calculation. J Alloys Compd 739:1080–1088. https://doi.org/10.1016/j.jallcom.2017.12.344
12. Jain A, Bhargava R, Poddar P (2013) Probing interaction of Gram-positive and Gram-negative bacterial cells with ZnO nanorods. Mater Sci Eng C 33:1247–1253. https://doi.org/10.1016/j.msec.2012.12.019
13. Mao H, Zhang B, Nie Y et al (2021) Enhanced antibacterial activity of V-doped ZnO@SiO_2 composites. Appl Surf Sci. https://doi.org/10.1016/j.apsusc.2021.149127
14. Sikam P, Takahashi K, Roongcharoen T et al (2021) Effect of 3d-transition metals doped in ZnO monolayers on the CO_2 electrochemical reduction to valuable products: first principles study. Appl Surf Sci. https://doi.org/10.1016/j.apsusc.2021.149380
15. Kutlu-Narin E, Narin P, Yildiz A, Lisesivdin SB (2020) Effects of annealing under different atmospheres on structural and optical properties of USCVD grown ZnO nanostructures. Mater Sci Eng B Solid State Mater Adv Technol. https://doi.org/10.1016/j.mseb.2020.114506
16. Talebian N, Amininezhad SM, Doudi M (2013) Controllable synthesis of ZnO nanoparticles and their morphology-dependent antibacterial and optical properties. J Photochem Photobiol B Biol 120:66–73. https://doi.org/10.1016/j.jphotobiol.2013.01.004
17. Sbardella F, Lilli M, Seghini MC et al (2021) Interface tailoring between flax yarns and epoxy matrix by ZnO nanorods. Compos Part A Appl Sci Manuf. https://doi.org/10.1016/j.compositesa.2020.106156
18. Xu Z, Zhu Y, Pang Z, Ge M (2021) Sol–gel preparation and properties of electroconductive Sn–Al co-doped ZnO coated TiO_2 whisker and its applications in textiles. Mater Sci Semicond Process. https://doi.org/10.1016/j.mssp.2020.105607
19. Vinoth V, Subramaniyam G, Anandan S et al (2021) Non-enzymatic glucose sensor and photocurrent performance of zinc oxide quantum dots supported multi-walled carbon nanotubes. Mater Sci Eng B Solid State Mater Adv Technol. https://doi.org/10.1016/j.mseb.2020.115036

20. Wilson DA, Gurung K, Langell MA (2021) Effect of zinc substitution on the growth morphology of ZnO–CuO tenorite solid solutions. J Cryst Growth. https://doi.org/10.1016/j.jcrysgro.2021.126062
21. Vasile OR, Serdaru I, Andronescu E et al (2015) Influence of the size and the morphology of ZnO nanoparticles on cell viability. Comptes Rendus Chim 18:1335–1343. https://doi.org/10.1016/j.crci.2015.08.005
22. Nethravathi PC, Shruthi GS, Suresh D et al (2015) Garcinia xanthochymus mediated green synthesis of ZnO nanoparticles: photoluminescence, photocatalytic and antioxidant activity studies. Ceram Int 41:8680–8687. https://doi.org/10.1016/j.ceramint.2015.03.084
23. Anbuvannan M, Ramesh M, Viruthagiri G et al (2015) Anisochilus carnosus leaf extract mediated synthesis of zinc oxide nanoparticles for antibacterial and photocatalytic activities. Mater Sci Semicond Process 39:621–628. https://doi.org/10.1016/j.mssp.2015.06.005
24. Thema FT, Manikandan E, Dhlamini MS, Maaza M (2015) Green synthesis of ZnO nanoparticles via *Agathosma betulina* natural extract. Mater Lett 161:124–127. https://doi.org/10.1016/j.matlet.2015.08.052
25. Anbuvannan M, Ramesh M, Viruthagiri G et al (2015) Synthesis, characterization and photocatalytic activity of ZnO nanoparticles prepared by biological method. Spectrochim Acta Part A Mol Biomol Spectrosc 143:304–308. https://doi.org/10.1016/j.saa.2015.01.124
26. Mateos-Pedrero C, Silva H, Pacheco Tanaka DA et al (2015) CuO/ZnO catalysts for methanol steam reforming: the role of the support polarity ratio and surface area. Appl Catal B Environ 174–175:67–76. https://doi.org/10.1016/j.apcatb.2015.02.039
27. Wong YR, Yuan Y, Du H, Xia X (2015) Development of high sensitivity, large frequency bandwidth ZnO-based accelerometers. Sens Actuators A Phys 229:23–29. https://doi.org/10.1016/j.sna.2015.03.012
28. Vandebriel RJ, De Jong WH (2012) A review of mammalian toxicity of ZnO nanoparticles. Nanotechnol Sci Appl 5:61–71
29. Hessien M, Da'na E, Taha A (2021) Phytoextract assisted hydrothermal synthesis of ZnO–NiO nanocomposites using neem leaves extract. Ceram Int 47:811–816. https://doi.org/10.1016/j.ceramint.2020.08.192
30. Karthikeyan C, Varaprasad K, Akbari-Fakhrabadi A et al (2020) Biomolecule chitosan, curcumin and ZnO-based antibacterial nanomaterial, via a one-pot process. Carbohydr Polym. https://doi.org/10.1016/j.carbpol.2020.116825
31. Duc Chinh N, Haneul Y, Minh Hieu N et al (2021) pn-Heterojunction of the SWCNT/ZnO nanocomposite for temperature dependent reaction with hydrogen. J Colloid Interface Sci 584:582–591. https://doi.org/10.1016/j.jcis.2020.10.017
32. Swamy MM, Surendra BS, Mallikarjunaswamy C et al (2021) Bio-mediated synthesis of ZnO nanoparticles using Lantana Camara flower extract: its characterizations, photocatalytic, electrochemical and anti-inflammatory applications. Environ Nanotechnol Monit Manag. https://doi.org/10.1016/j.enmm.2021.100442
33. Rai P, Yu YT (2012) Citrate-assisted hydrothermal synthesis of single crystalline ZnO nanoparticles for gas sensor application. Sens Actuators B Chem 173:58–65. https://doi.org/10.1016/j.snb.2012.05.068
34. Kumar SG, Kavitha R, Sushma C (2020) Doped zinc oxide nanomaterials: structure–electronic properties and photocatalytic applications. In: Interface science and technology, Elsevier B.V., pp 285–312
35. Mukhtar F, Munawar T, Nadeem MS et al (2021) Dual S-scheme heterojunction ZnO–V_2O_5–WO_3 nanocomposite with enhanced photocatalytic and antimicrobial activity. Mater Chem Phys. https://doi.org/10.1016/j.matchemphys.2021.124372
36. Zhao S, Liu T, Zhang Y et al (2016) Cr-doped MnO_2 nanostructure: morphology evolution and electrochemical properties. J Mater Sci Mater Electron 27:3265–3270. https://doi.org/10.1007/s10854-015-4154-1
37. Karthikeyan C, Varaprasad K, Venugopal SK et al (2021) Biocidal (bacterial and cancer cells) activities of chitosan/CuO nanomaterial, synthesized via a green process. Carbohydr Polym 259:117762. https://doi.org/10.1016/j.carbpol.2021.117762
38. Keshari AK, Gupta P, Singh M (2021) ZnO nanoparticles doping with transition metal elements in polymeric and biomacromolecular matrix and their optical evolution. Opt Mater (Amst) 111:110697. https://doi.org/10.1016/j.optmat.2020.110697
39. Kamboh MA, Wang H, Wang L et al (2021) Ab initio study of the thermodynamic, electronic and optical properties of WC (Bh) phase ZnO under pressure. Mater Sci Eng B Solid State Mater Adv Technol. https://doi.org/10.1016/j.mseb.2020.115008
40. Iwamoto M, Manaka T (2010) Probing and modeling of carrier motion in organic devices by optical second harmonic generation. In: Thin solid films, pp 961–963
41. Shah Saqib AN, Thu Huong NT, Kim SW et al (2021) Structural and magnetic properties of highly Fe-doped ZnO nanoparticles synthesized by one-step solution plasma process. J Alloys Compd 853:157153. https://doi.org/10.1016/j.jallcom.2020.157153
42. Siva N, Sakthi D, Ragupathy S et al (2020) Synthesis, structural, optical and photocatalytic behavior of Sn doped ZnO nanoparticles. Mater Sci Eng B Solid State Mater Adv Technol 253:114497. https://doi.org/10.1016/j.mseb.2020.114497
43. Tan M, Qiu G, Ting YP (2015) Effects of ZnO nanoparticles on wastewater treatment and their removal behavior in a membrane bioreactor. Bioresour Technol 185:125–133. https://doi.org/10.1016/j.biortech.2015.02.094
44. Bandyopadhyay S, Plascencia-Villa G, Mukherjee A et al (2015) Comparative phytotoxicity of ZnO NPs, bulk ZnO, and ionic zinc onto the alfalfa plants symbiotically associated with *Sinorhizobium meliloti* in soil. Sci Total Environ 515–516:60–69. https://doi.org/10.1016/j.scitotenv.2015.02.014
45. Sharma D, Rajput J, Kaith BS, et al (2010) Synthesis of ZnO nanoparticles and study of their antibacterial and antifungal properties. In: Thin solid films, Elsevier, pp 1224–1229
46. Sha S, Hou Q, Liu Y, Qi M (2021) Effects of different valence states of Mo and point vacancies on magneto-optical properties of ZnO. Phys B Condens Matter. https://doi.org/10.1016/j.physb.2020.412485
47. Khan MI, Fatima N, Shakil M et al (2021) Investigation of in-vitro antibacterial and seed germination properties of green synthesized pure and nickel doped ZnO nanoparticles. Phys B Condens Matter 601:412563. https://doi.org/10.1016/j.physb.2020.412563
48. Okeke IS, Agwu KK, Ubachukwu AA et al (2021) Impact of particle size and surface defects on antibacterial and photocatalytic activities of undoped and Mg-doped ZnO nanoparticles, biosynthesized using one-step simple process. Vacuum 187:110110. https://doi.org/10.1016/j.vacuum.2021.110110
49. Worku AK, Ayele DW, Habtu NG (2021) Recent advances and future perspectives in engineering of bifunctional electrocatalysts for rechargeable zinc–air batteries. Mater Today Adv 9:100116. https://doi.org/10.1016/j.mtadv.2020.100116
50. Mandal H, Shyamal S, Hajra P et al (2014) Improved photoelectrochemical water oxidation using wurtzite ZnO semiconductors synthesized through simple chemical bath reaction. Electrochim Acta 141:294–301. https://doi.org/10.1016/j.electacta.2014.06.013

51. Sun L, Shao Q, Zhang Y et al (2020) N self-doped ZnO derived from microwave hydrothermal synthesized zeolitic imidazolate framework-8 toward enhanced photocatalytic degradation of methylene blue. J Colloid Interface Sci 565:142–155. https://doi.org/10.1016/j.jcis.2019.12.107
52. Aboulaich A, Tilmaciu CM, Merlin C et al (2012) Physicochemical properties and cellular toxicity of (poly) aminoalkoxysilanes-functionalized ZnO quantum dots. Nanotechnology. https://doi.org/10.1088/0957-4484/23/33/335101
53. Geetha MS, Nagabhushana H, Shivananjaiah HN (2016) Green mediated synthesis and characterization of ZnO nanoparticles using Euphorbia Jatropa latex as reducing agent. J Sci Adv Mater Devices 1:301–310. https://doi.org/10.1016/j.jsamd.2016.06.015
54. Ahmad I, Akhtar MS, Manzoor MF et al (2020) Synthesis of yttrium and cerium doped ZnO nanoparticles as highly inexpensive and stable photocatalysts for hydrogen evolution. J Rare Earths. https://doi.org/10.1016/j.jre.2020.04.002
55. Gorgulla A, Ertel DP, Steyer M, et al (2015) Effect of Al concentration analyzed by ICP-OES on the structural, electrical and optical properties of Co-sputtered ZnO:Al films. In: Energy procedia, Elsevier Ltd, pp 687–693
56. Bandeira M, Possan AL, Pavin SS et al (2020) Mechanism of formation, characterization and cytotoxicity of green synthesized zinc oxide nanoparticles obtained from Ilex paraguariensis leaves extract. Nano Struct Nano Obj. https://doi.org/10.1016/j.nanoso.2020.100532
57. Panchal P, Paul DR, Sharma A et al (2020) Biogenic mediated Ag/ZnO nanocomposites for photocatalytic and antibacterial activities towards disinfection of water. J Colloid Interface Sci 563:370–380. https://doi.org/10.1016/j.jcis.2019.12.079
58. Alamelu K, Jaffar Ali BM (2020) Ag nanoparticle-impregnated sulfonated graphene/TiO_2 composite for the photocatalytic removal of organic pollutants. Appl Surf Sci 512:145629. https://doi.org/10.1016/j.apsusc.2020.145629
59. Sagadevan S, Vennila S, Lett JA et al (2019) Tailoring the structural, morphological, optical, thermal and dielectric characteristics of ZnO nanoparticles using starch as a capping agent. Results Phys 15:102543. https://doi.org/10.1016/j.rinp.2019.102543

Publisher's Note Springer Nature remains neutral with regard to jurisdictional claims in published maps and institutional affiliations.